

Article

Effect of Photoanode Process Sequence on Efficiency of Dye-Sensitized Solar Cells

Tian-Chiuan Wu, Wei-Ming Huang, Jenn-Kai Tsai * , Cheng-En Chang and Teen-Hang Meen * 

Department of Electronic Engineering, National Formosa University, Yunlin 632, Taiwan; eetcwu@nfu.edu.tw (T.-C.W.); 11060119@gm.nfu.edu.tw (W.-M.H.); en11160137@gmail.com (C.-E.C.)
* Correspondence: tsajk@nfu.edu.tw (J.-K.T.); thmeen@gs.nfu.edu.tw (T.-H.M.)

Abstract: Owing to its contribution to carbon emission reduction, green energy has received widespread attention. Among green energy sources, solar energy is regarded as the most important. In solar energy production, dye-sensitized solar cells (DSSCs) have been favored owing to their characteristics of simple manufacturing and high efficiency as a third-generation solar cell technology. DSSCs are prospective candidates for powering indoor Internet of Things (IoT) devices. In this study, to find a method to enhance DSSCs' efficiency, the advantages and disadvantages of the screen printing method and the mechanical pressing and annealing method were analyzed. Using an improved method, a TiO₂ photoanode was processed and annealed, and the DSSCs with the photoanode showed an efficiency increase from 1.10 to 4.78%.

Keywords: dye-sensitized solar cells; screen printing; pressing; annealing

1. Introduction

Since the Industrial Revolution in the 19th century, the progress of human civilization has been accelerated but has required a largely increased demand for energy. Previously, the main energy sources were mainly fossil fuels such as coal, oil, and natural gas [1,2]. However, the combustion of fossil fuels emits greenhouse gases such as carbon dioxide, which has changed the global climate abnormally. To mitigate the impact of global climate change and transition to a sustainable future, the use of renewable energy is an unavoidable choice. Among various renewable energies, solar energy is regarded as the most promising and transformative source, as it has proven its cost-effectiveness and environmentally friendliness. In addition, solar energy does not produce harmful greenhouse gases or pollutants.

In using solar energy, dye-sensitized solar cells (DSSCs) have attracted widespread attention and interest because of their low preparation costs and minimal equipment requirements compared to Si-based solar cells. Thus, a DSSC is a viable choice for solar energy production. However, more research and developments are required to improve the conversion efficiency of DSSCs to enhance their feasibility and competitiveness in energy production. If the conversion efficiency of DSSCs is increased to higher levels than before, the potential of DSSCs will contribute to securing energy accessibility, especially in developing countries. The low-cost preparation and minimal equipment requirements of a DSSC make it an attractive option in countries for which financial and technical resources are important. Solar energy production using DSSCs allows developing countries to harness solar power for energy security independently, economic development, and reduced carbon emissions worldwide. These initiatives also align with the seventh vision of the Sustainable Development Goals (SDGs) launched by the United Nations. By developing and deploying such advanced solar technologies, environmental issues can be solved with broader socioeconomic goals achieved, which will bring a more sustainable and equitable future. Advanced solar technologies, such as DSSCs, are important to balance human progress and environmental protection in harmony.



Citation: Wu, T.-C.; Huang, W.-M.; Tsai, J.-K.; Chang, C.-E.; Meen, T.-H. Effect of Photoanode Process Sequence on Efficiency of Dye-Sensitized Solar Cells. *Coatings* **2024**, *14*, 304. <https://doi.org/10.3390/coatings14030304>

Academic Editor: Alessandro Latini

Received: 8 February 2024

Revised: 24 February 2024

Accepted: 27 February 2024

Published: 29 February 2024



Copyright: © 2024 by the authors. Licensee MDPI, Basel, Switzerland. This article is an open access article distributed under the terms and conditions of the Creative Commons Attribution (CC BY) license (<https://creativecommons.org/licenses/by/4.0/>).

In the fabrication of DSSCs, the titanium dioxide (TiO₂) layer may encounter issues such as a loose structure or cracks, depending on the preparation methods. Some scientists have addressed these concerns by optimizing the structure through the addition of binders or additives [3]. In this study, mechanical pressurization and annealing processes were employed to enhance the structure of the TiO₂ nanoparticle (NP) layer and subsequently increase the power conversion efficiency (PCE) [4,5]. The TiO₂ NP photoanode thin film is mechanically compressed before being thermally treated to produce a uniform and smooth compressed film and improve electron transport between the NPs. The film becomes uniform and dense as the mechanical compression transforms the porous structure of the mesoporous TiO₂ NP layer into a dense structure in the compressed TiO₂ NP layer. Therefore, electrolyte penetration into the fluorine-doped tin oxide (FTO) substrate is prevented, and charge recombination is reduced. Such a mechanism has been validated by using porosity measurements and open-circuit voltage decay measured with electrochemical impedance spectroscopy and scanning electron microscopy (SEM). The compressed film reduces porosity, improves particle connectivity, enhances transparency, and increases the power conversion efficiency (PCE) [6,7]. However, although the structure is dense, dye molecules can still permeate through the TiO₂ NPs and adhere to their surfaces. The resulting high light transmission rate of the TiO₂ NP thin film decreases absorbance at wavelengths longer than 560 nm. Therefore, compression has been used as an effective method to fabricate crack-free and high-quality TiO₂ NP thin films for high-performance DSSCs [4,5].

The doctor blade method is a cost-effective, flexible, and simple physical deposition method for the low-temperature fabrication of a flexible DSSC [8]. In this method, a photoanode paste is applied to the substrate before being spread with a doctor's blade or a glass rod. However, the doctor blade method may introduce errors due to the instability of human operation. Another low-temperature fabrication method for flexible DSSCs is screen printing. Screen printing is widely used owing to the abundant availability of printable pastes, its scalability for mass production [9], and its suitability for fabricating thin films. The thickness of DSSCs is easily controlled by easily varying the thickness of the paste [10].

Therefore, FTO is used as the glass substrate in this study, as common indium tin oxide (ITO) reduces its conductivity after high-temperature annealing. FTO can be heated up to 500 °C while maintaining a stable low resistance in two-step annealing: at 150 °C for 90 min and then at 500 °C for 30 min to form TiO₂ photoanodes [4,5]. Residual organic compounds are decomposed in annealing at 150 °C, while TiO₂ nanoparticles (NPs) are interconnected at 500 °C, thereby reducing the electron transport loss [11]. Annealing TiO₂ thin films significantly changes the carrier concentration and electrical conductivity and enhances the separation of holes and electrons [12]. Such annealing effectively generates oxygen vacancies on the surface of TiO₂ and enhances light absorption and the separation of charge carriers. At the same time, annealing allows TiO₂ nanoparticles to have closer contact to shorten the path for photogenerated charges to transfer to the substrate. This separates and transfers charge carriers more effectively, resulting in a substantial transfer of holes to the substrate [13].

Previously, pressurization and annealing effects had been separately explored. Therefore, it is required to explore the advantages and disadvantages of their impacts on the PCE of DSSCs at the same time. Thus, we studied the effects of pressurization and annealing on a DSSC with a TiO₂ film to maximize the PCE.

2. Materials and Methods

2.1. Materials

FTO substrates (7 Ω/sq) and ITO substrates (7 Ω/sq) were purchased from Ruilong, Miaoli, Taiwan. Acetone (95%), tertbutanol alcohol (99%), ethanol (95%), ethanol (99%), tert-butanol (99%), n-pentane (99%), and methyl alcohol (95%) were purchased from UNIONWARD Corp., New Taipei, Taiwan. Lithium iodide (LiI, 98%) was made by Alfa Aesar, Ward Hill, MA, USA. Iodide (I₂, 99.8%) was manufactured by Sigma-Aldrich, Bangalore,

India. 4-tertbutylpyridine (TBP, 99%) was manufactured by Sigma-Aldrich, Burlington, MA, USA. Titanium dioxide P25 powder (TiO₂ P25, anatase 80% and rutile 20%, size 20 nm) was purchased from UniRegion Bio-Tech, New Taipei, Taiwan. Acetonitrile (99.5%) was manufactured by Avantor Performance Materials, Radnor, PA, USA. 3-methoxypropionitrile (MPN, 99%) was purchased from FLUKA, Charlotte, NC, USA. Surlyn films were purchased from C.P SOLAR, Kaohsiung, Taiwan. 1,2-dimethyl-3-propylimidazolium iodide (DMPII, 98%) was purchased from TCI, Tokyo, Japan.

2.2. Fabrication

2.2.1. Substrate Cleaning

Firstly, the FTO substrates were treated with acetone, methanol, and deionized water in sequence for 5 min with an ultrasonic cleaner and then dried using a nitrogen blower gun. Before coating, the FTO substrate was cleaned with an ultraviolet ozone (UVO) cleaner for 10 min.

2.2.2. TiO₂ Paste Preparation

The paste for screen printing was prepared from a mixture of tertiary butanol, anhydrous alcohol, and TiO₂ P25, where the concentration of TiO₂ P25 was 10 wt% (1.2446 g), and the ratio of tert-butanol to anhydrous alcohol was 2:1 (6 mL, 3 mL).

2.2.3. N3 Dye Preparation

The N3 dye solution was prepared by mixing N3 powder with a combination of tert-butanol and acetonitrile in a 1:1 volume ratio, resulting in a concentration of 3×10^{-4} M.

2.2.4. Electrolyte Preparation

The electrolyte was prepared by mixing 0.05 M of I₂, 0.1 M of LiI, 0.5 M of TBP, and 1 M of DMPII. The mixture was then poured into MPN and finally thoroughly mixed using an ultrasonic cell disruptor to complete the preparation of the electrolyte.

2.2.5. Photoanode Preparation

In the screen printing, we used tetoron with a mesh count of 150 and an effective area of 0.25 cm² as the screen material. The FTO substrate was coated 4 times via screen printing to obtain mesoporous TiO₂ films. The prepared mesoporous TiO₂ films were divided into four types based on the presence or absence of pressurization and annealing processes. These include the TiO₂ layer without annealing or pressurization (N), the annealed TiO₂ layer (A), the pressurized TiO₂ layer (P), and the pressurized and annealed TiO₂ layer (PA). The process sequence involved pressurization followed by annealing. The TiO₂ films were pressurized using a hydraulic press machine. The pressure condition of the TiO₂ films was 138.4 kg/cm² for 60 s [5]. The TiO₂ film was annealed in two steps. First, it was heated to 150 °C for 1.5 h and then annealed at 450 °C for 30 min.

The prepared TiO₂ film was soaked in the N3 dye solution and kept at 45 °C for 2 h to prepare the photoanode.

2.2.6. Counter Electrode Preparation

ITO served as the substrate. Initially, the ITO substrate underwent perforation to create channels for the injection of the electrolyte during the sealing process. Following this, the substrate underwent a cleaning procedure, adhering to the steps outlined in Section 2.2.1. After completion of the cleaning process, platinum was deposited onto the cleaned ITO substrate using sputtering deposition techniques. The sputtering parameters were 10 mA for 60 s under an argon atmosphere.

2.2.7. DSSC Device Encapsulation

The photoanode and counter electrode were assembled into a sandwich structure using a heat-shrinkable film. Subsequently, the electrolyte was injected into the structure

through the holes on the counter electrode. Finally, the holes on the counter electrode were sealed using a heat-shrinkable film and small pieces of glass.

2.3. Characterization

The photoanode film's morphology was examined with a Field Emission Scanning Electron Microscope (FE SEM, JSM 7610FPlus, JEOL, Tokyo, Japan). A UV–visible spectrometer (U2900A, Hitachi, Tokyo, Japan) was used to measure the visible light absorption of the photoanode film in the DSSC. The crystalline phase of TiO₂ was analyzed through X-ray diffraction metrology (XRD) (D8, BRUKER, Billerica, MA, USA). The power conversion efficiency of the DSSC was determined using a solar simulator (XES 40S1, San Ei Brand, Osaka, Japan) under AM 1.5 (100 mW/cm²). Electrochemical impedance spectroscopy (EIS) (Zennium, Zahner, Kronach, Germany) was used to measure the impedance of the DSSC.

3. Results and Discussions

3.1. SEM Analysis

Figure 1 shows the cross-sectional SEM images of the TiO₂ layer prepared by screen printing. In the figure, the as-deposited TiO₂ layer without annealing and pressurization processes, the annealed TiO₂ layer, the pressurized TiO₂ layer, and the pressurized and annealed TiO₂ layer are presented in Figure 1a–d, respectively. The thickness of the TiO₂ film was approximately 30–40 μm and showed many cracks and a loose structure (Figure 1a,b). The difference in thickness between the N and A samples was not clearly obvious because the organic solvents evaporated when the FESEM images of the two samples were taken. The structural collapse was caused by the rapid evaporation of the organic solvents, which formed cracks on the films. The collapse and thickness reduction of the structure were attributed to the rapid evaporation of organic solvents in the annealing process. This porous structure increases the dye adsorption capacity and enhances the generation of photoelectrons, thereby boosting the current [14]. However, this structure has drawbacks such as a longer pathway for electron transfer and direct contact between the electrolyte and the FTO substrate. These disadvantages increase electron recombination before they are transferred to the external circuit, reducing the efficiency [15].

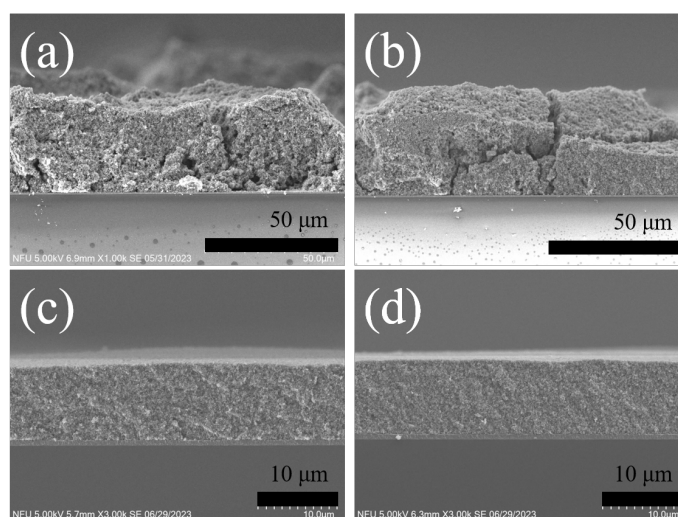


Figure 1. The cross-section SEM images of the TiO₂ layer fabricated by screen printing. (a) As-deposited TiO₂ layer without annealing and pressurization, (b) annealed TiO₂ layer, (c) pressurized TiO₂ layer, and (d) TiO₂ layer subjected to both pressurization and annealing. The scale bar in (a,b) presents a length of 50 μm, while that in (c,d) is 10 μm.

The thickness of the TiO₂ film was approximately 9–10 μm (Figure 1c,d). Compared to Figure 1a,b, it was found that the pressurization significantly reduced the thickness of the film, forming a more compact structure. This structure considerably shortened the

pathway for electron transfer, facilitating electron transport. This dense structure prevents direct contact between the electrolyte and the FTO substrate [16–18]. However, due to this compact structure, fewer photogenerated electrons were generated, with a smaller dye adsorption capacity than that of the DSSCs without pressurization.

A distinct array structure was observed on the surface of the TiO₂ film prepared by the screen-printing method (Figure 2a). The structure size was determined by the mesh size. Several blocks within the array exhibited no structures due to screen lift during the screen printing. The screen lift made the pastes adhere to the screen instead of the film and caused a loss of block structure. This resulted in direct contact between the electrolyte and the FTO substrate over a larger area. Figure 2c,d show that the surface of the TiO₂ film became smooth after pressurization. Such smoothness explained the significant difference in thickness between the film before and after pressurization (reduced from 30–40 to 9–10 μm). The original block structure gradually disappeared into the surroundings, filling the voids and consequently reducing the film thickness.

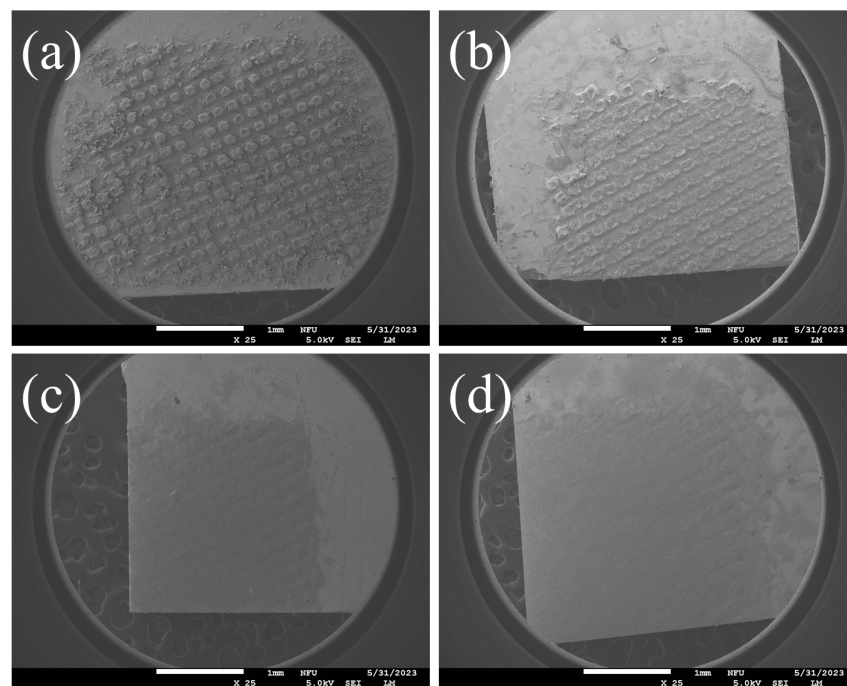


Figure 2. The top-view SEM images of the TiO₂ layer prepared by screen printing. (a) TiO₂ layer without annealing and pressurization, (b) annealed TiO₂ layer, (c) pressurized TiO₂ layer, and (d) TiO₂ layer subjected to both pressurization and annealing.

3.2. XRD Analysis

Figure 3 shows the XRD patterns of the four types of TiO₂ layers: the TiO₂ layer without annealing and pressurization (N), the annealed TiO₂ layer (A), the pressurized TiO₂ layer (P), and the pressurized and annealed TiO₂ layer (PA). The four types of TiO₂ layers showed similar characteristics in terms of peaks, indicating that the crystalline phase of TiO₂ remained unchanged regardless of pressurization or annealing. Such consistency helped to maintain the same ratio of the rutile phase and the anatase phase of TiO₂ [19,20].

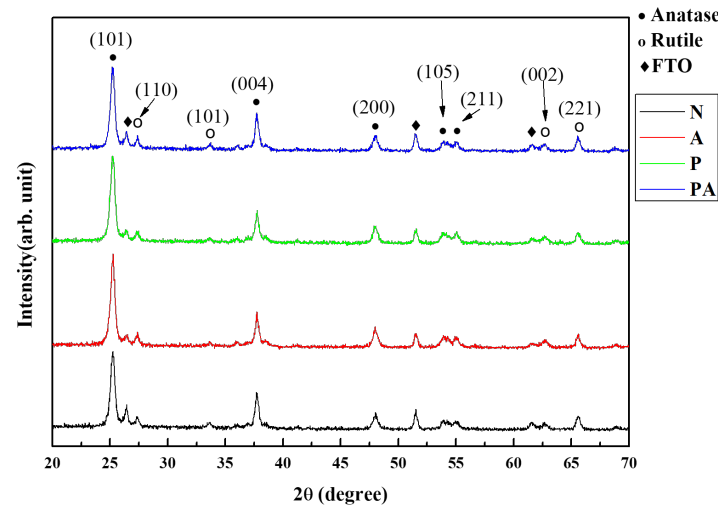


Figure 3. The XRD patterns of the TiO₂ layer. The TiO₂ layer without annealing and pressurization (N), the annealed TiO₂ layer (A), the pressurized TiO₂ layer (P), and the TiO₂ layer that has been pressurized and annealed (PA). (JCPDS card no. 21-1272).

3.3. UV-Vis Analysis

Figure 4 shows the UV-Vis absorption spectra of the four types of TiO₂ layers. The absorbance is equal to $\log(I_0/I)$, where I_0 is the incident light and I is the transmitted light. N and A showed better absorbance at visible light wavelengths than in the near-infrared light wavelength range due to the loose structure of the TiO₂ layer. The loose structure resulted in more light absorption. In contrast, P and PA, with pressurized TiO₂ layers, showed decreased absorbance at visible and near-infrared wavelengths. As the pressurized film was thin, light with a long wavelength easily passed through the film. The pressurized TiO₂ layers (P and PA) showed much lower absorbances than N and A.

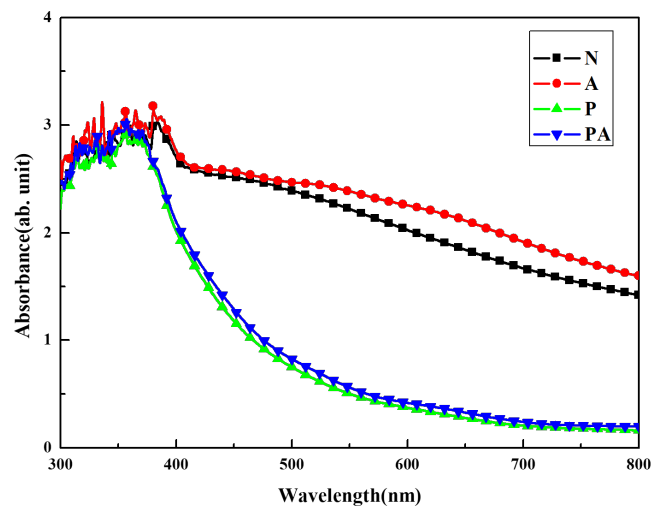


Figure 4. The absorbance of the four types of TiO₂ layers.

Figure 5 shows the TiO₂ layers after dye soaking (a) without compression and (b) with compression. The TiO₂ layer without compression appears darker in color, whereas the compressed TiO₂ layer appears brighter under indoor lighting. That is, the compressed TiO₂ layer exhibits better transparency. Because light with a long wavelength is less likely to be scattered, it is more likely to penetrate the photoanode layer. This is why the sample appears reddish to the naked eye.

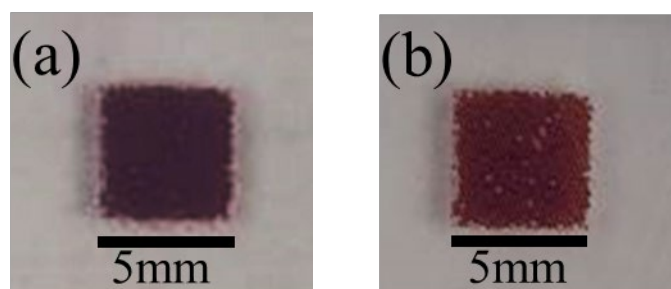


Figure 5. The TiO₂ layer after dye immersion: (a) without compression and (b) with compression.

Figure 6 shows the UV-Vis absorption spectra of four types of TiO₂ layers after the treatment with N3 dye. The difference in absorbance between the TiO₂ layers with un-adsorbed and adsorbed dye is proportional to the amount of adsorbed dye. Although the exact amount of adsorbed dye could not be measured, the difference in adsorption between them could be inferred by comparing the same TiO₂ layer before and after dye immersion and determining the dye adsorption capacity. The absorbance of N and A kept increasing from 300 to 550 nm, while that of P and PA increased to 400 nm but then rapidly decreased to 800 nm. This occurred due to the presence of N3 dye. This confirms the successful absorption of the dye by the photoanodes. Before the treatment with the N3 dye, the absorbance at 550 nm for N, A, P, and PA was 2.34, 2.33, 0.76, and 0.59, respectively. After the treatment, the absorbances increased to 3.67, 3.54, 1.69, and 1.49, respectively. The degree of dye absorption was determined by calculating the ratio of I_0/I . The degrees of dye adsorption of N, A, PA, and P were 21.23, 16.22, 8.53, and 7.98. N and A exhibited more increases in absorbance due to their loose structure and adhesion to dye molecules. The smaller increase in the absorbance of A than N was caused by the binding between nanoparticles after annealing, resulting in less dye adsorption. The increase in absorbance for P and PA was expected to be higher than the measurement results as they had a denser structure than N and A. The close contact between the nanoparticles resulted in less surface area for the adsorption of the dye molecules, leading to less dye adsorption. In summary, the pressurized TiO₂ had a lower degree of dye adsorption, which reduced dye consumption and costs in fabrication.

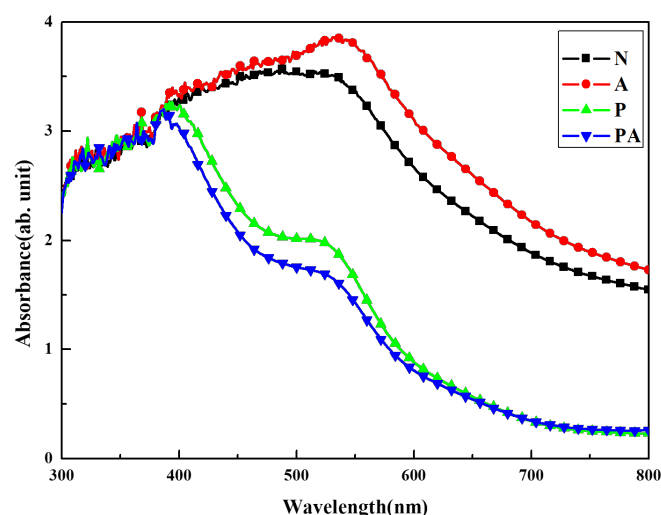


Figure 6. The UV-Vis absorbance spectra of four types TiO₂ layers after soaking in dye.

3.4. EIS Characteristics

We measured the derived resistances and parameters of the fabricated DSSCs using an Nyquist diagram: R_S (series resistance of wires and bulk), R_{PT} (related to electrochemical reactions at the platinum counter electrode and electrolyte interface), R_D (associated with

the Warburg diffusion process of I^-/I_3^- in the electrolyte), R_K (representing charge transport through the TiO_2 , dye, and electrolyte interfaces), τ_{eff} (electron lifetime), and K_{eff} (electronic recombination rate constant) (results shown in Table 1 and Figure 7). To calculate K_{eff} , we identified the highest point in the mid-frequency region, corresponding to the frequency of that point. K_{eff} is subsequently used in the equation $\tau_{eff} = 1/2\pi K_{eff}$ to determine τ_{eff} [21].

Table 1. The EIS characteristics of DSSCs with four different photoanodes.

Sample	R_S (Ω)	R_{PT} (Ω)	R_K (Ω)	R_D (Ω)	K_{eff} (s^{-1})	τ_{eff} (s)
N	13.72	N/A	122.45	10.62	106.61	1.493
A	16.79	3.38	13.85	4.06	19.37	8.217
P	16.20	5.48	14.91	6.33	32.77	4.856
PA	12.96	3.26	14.82	8.42	19.37	8.217

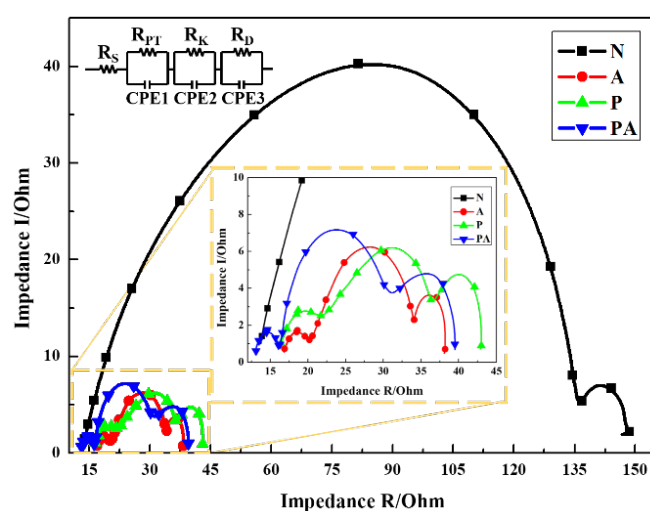


Figure 7. The Nyquist plot of DSSCs with four different photoanodes.

In the Nyquist diagram of the DSSCs, three capacitances were represented, including CPE1 (interface capacitance at the platinum counter electrode and electrolyte interface), CPE2 (interface capacitance at the TiO_2 , dye, and electrolyte interfaces), and CPE3 (constant phase element related to charge transport through the TiO_2 , dye, and electrolyte interfaces). The impedance, R_K , and τ_{eff} of the photoanodes of the DSSCs were measured. Due to the R_K resistance value rose too fast, causing the semicircle of the R_{PT} to be covered and calculation could not be performed, so the R_{PT} was marked as N/A. increased too rapidly to calculate. A significant difference in R_K between N and A was also observed. Annealing caused a difference of 88.7% in R_K (decreased from 122.45 to 13.85 Ω). K_{eff} also decreased significantly by 82% from 106.61 to 19.37 s^{-1} . This indicates that annealing improved electron transmission and reduced the probability of electron recombination. The impact of pressurization was evident when comparing the parameters of N with those of P. After pressurization, R_K decreased by 87.8% from 122.45 to 14.91, and K_{eff} also decreased by 69% from 106.61 to 32.77 s^{-1} . This confirms the reduction in film thickness and the electron transmission path after pressurization, as well as the improved electron transmission rate and probability of electron recombination. PA showed the advantages of pressurization and annealing, demonstrating the lowest R_K (14.82 Ω) and K_{eff} (19.37 s^{-1}). PA showed the highest PCE.

3.5. J-V Characteristics

The J-V characteristics of the DSSCs with the photoanodes are presented in Figure 8 and Table 2. The short-circuit current (I_{SC}) was recorded at a measured voltage of 0. Subsequently, the short-circuit current density (J_{SC}) was calculated by dividing I_{SC} by

the photoanode area. The open-circuit voltage (V_{OC}) was recorded when the measured current reached 0 at a certain voltage level. The product of the measured current and voltage at its maximum point was obtained as the maximum power output (P_{max}), with its corresponding current density (J_{max}) and voltage (V_{max}). The fill factor (F.F.) represents the device's capability to provide the maximum output power and is calculated as the ratio of P_{max} to the product of V_{OC} and J_{SC} . The photovoltaic conversion efficiency (PCE) is determined by multiplying V_{OC} , J_{SC} , and F.F. and then dividing the result by the incident light power (100 mW/cm^2).

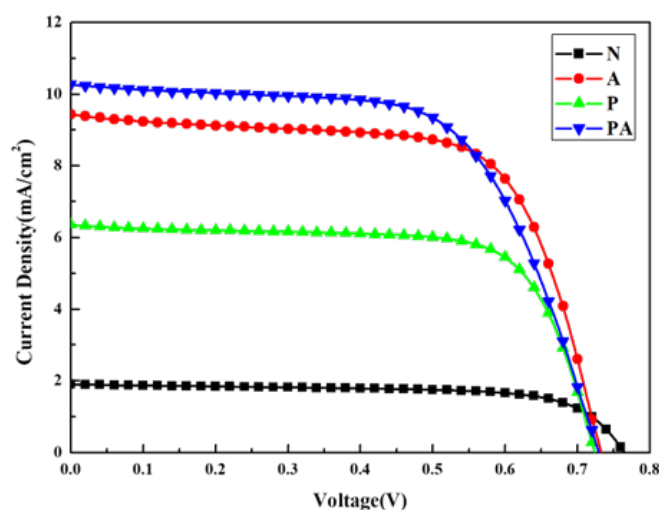


Figure 8. The J-V characteristics curve of DSSCs with our different photoanodes.

Table 2. The J-V characteristics of DSSCs with four different photoanodes.

Sample	V_{OC} (V)	J_{SC} (mA/cm^2)	Fill Factor (%)	PCE (%)
N	0.77	1.91	69.22	1.01
A	0.73	9.44	67.55	4.67
P	0.72	6.36	71.46	3.29
PA	0.73	10.27	63.17	4.73

From Table 2, N has the lowest PCE, but its V_{OC} is the highest among the four samples. We believe that, under the same light intensity, sample N with more dye adsorption should produce more electron–hole pairs. The impedance of its photoanode is higher, so it is not easy for the photoelectrons to be transmitted, and finally, the electron holes must be recombined in the photoanode. This results in a lower short-circuit current than the other samples. In the open circuit, the external voltage prevents the photoelectrons from traveling through the photoanode, and the higher impedance likely makes electron holes recombine more slowly than in the other samples, resulting in higher open-circuit voltages. A exhibited the second-highest J_{SC} , which was 4.68 times higher than the J_{SC} of N (from 1.01% to 4.67%). This was attributed to the enhanced contact between the TiO_2 nanoparticles after annealing, which promoted particle fusion, reduced the contact interface between the nanoparticles, and improved electron transport. P showed a significant improvement in the PCE, which was 3.26 times higher than that of N (from 1.01% to 3.29%). Although pressurization was less favorable for PCE enhancement compared to annealing, it still had advantages of maintaining a low-temperature processes. In summary, pressurization contributed to an improvement in the PCE of the DSSC due to the flexible or ITO glass substrates. PA showed the advantages of pressurization and annealing together, having the optimal PCE.

4. Conclusions

In this study, a screen printing method was used to prepare a TiO₂ layer as the photoanode of DSSCs, and the structure and characteristics of the TiO₂ layer were improved with pressurization and annealing. The PCE of the DSSCs was also improved with pressurization and annealing. The structure of the TiO₂ layer was compacted with pressurization, and the electron transmission path was shortened, thereby reducing the electron recombination effect and improving the PCE. The process required less use of dyes, which saved on fabrication costs. Through annealing, the contact between the nanoparticles was limited, which reduced the interface resistance between the nanoparticles and improved the PCE. The DSSC based on the pressurized and annealed TiO₂ film showed the best PCE of 4.73%, which was 4.68 times higher than that of the DSSCs without these processes (1.01%). However, the DSSC with only pressurization or annealing did not exhibit a significantly improved PCE. Such results are expected to contribute considerably to improving the fabrication process, for instance, if the DSSC fabrication process needs to be conducted at a low temperature within a shorter time than previously, and pressurization is required to enhance the PCE of fabricated DSSCs. To save costs while maintaining good PCE, annealing can be introduced into the fabrication process. The results of this study provide a basis for developing the fabrication process of DSSCs to obtain the best PCE.

Author Contributions: FE-SEM measurement, T.-C.W.; W.-M.H. carried out the preparation of samples, UV-vis absorption, and J-V measurements; XRD measurement, C.-E.C.; EIS measurement, T.-H.M.; designed the work and editing the manuscript, J.-K.T. All authors have read and agreed to the published version of the manuscript.

Funding: This research received no external funding.

Institutional Review Board Statement: Not applicable.

Informed Consent Statement: Not applicable.

Data Availability Statement: Data is contained within the article.

Conflicts of Interest: The authors declare no conflict of interest.

References

1. Wang, Q.; Guo, J.; Li, R.; Jiang, X.T. Exploring the role of nuclear energy in the energy transition: A comparative perspective of the effects of coal, oil, natural gas, renewable energy, and nuclear power on economic growth and carbon emissions. *Environ. Res.* **2023**, *221*, 115290. [[CrossRef](#)]
2. Karim, N.A.; Mehmood, U.; Zahid, H.F.; Asif, T. Nanostructured photoanode and counter electrode materials for efficient DSSCs. *Sol. Energy* **2019**, *185*, 165–188. [[CrossRef](#)]
3. Ito, S.; Murakami, T.N.; Comte, P.; Liska, P.; Grätzel, C.; Nazeeruddin, M.K.; Grätzel, M. Fabrication of thin film dye sensitized solar cells with solar to electric power conversion efficiency over 10%. *Thin Solid Film.* **2008**, *516*, 4613–4619. [[CrossRef](#)]
4. Meen, T.H.; Tsai, J.K.; Tu, Y.S.; Wu, T.C.; Hsu, W.D.; Chang, S.-J. Optimization of the dye-sensitized solar cell performance by mechanical compression. *Nanoscale Res. Lett.* **2014**, *9*, 523. [[CrossRef](#)] [[PubMed](#)]
5. Tsai, J.K.; Hsu, W.D.; Wu, T.C.; Meen, T.H.; Chong, W.J. Effect of compressed TiO₂ nanoparticle thin film thickness on the performance of DSSCs. *Nanoscale Res. Lett.* **2013**, *8*, 459. [[CrossRef](#)] [[PubMed](#)]
6. Cao, D.; Wang, A.; Yu, X.; Yin, H.; Zhang, J.; Mi, B. Room-temperature preparation of TiO₂/graphene composite photoanodes for efficient dye-sensitized solar cells. *J. Colloid Interface Sci.* **2021**, *586*, 326–334. [[CrossRef](#)] [[PubMed](#)]
7. Dittrich, T.; Ofir, A.; Tirosh, S.; Grinis, L.; Zaban, A. Influence of the porosity on diffusion and lifetime in porous TiO₂ layers. *Appl. Phys. Lett.* **2006**, *88*, 182110. [[CrossRef](#)]
8. Ahmad, M.S.; Pandey, A.K.; Abd Rahim, N. Advancements in the development of TiO₂ photoanodes and its fabrication methods for dye-sensitized solar cell (DSSC) applications. A review. *Renew. Sustain. Energy Rev.* **2017**, *77*, 89–108. [[CrossRef](#)]
9. Liu, J.; Li, Y.; Arumugam, S.; Tudor, J.; Beeby, S. Investigation of low temperature processed titanium dioxide (TiO₂) films for printed dye-sensitized solar cells (DSSCs) for large area flexible applications. *Mater. Today Proc.* **2018**, *5*, 13846–13854. [[CrossRef](#)]
10. Husain, A.; Hasan, W.W. Transparent solar cell using spin coating and screen printing. *Pertanika J. Sci. Technol.* **2017**, *25*, 225–233.
11. Tsai, J.K.; Tu, Y.S. Fabrication of polymeric anti-reflection film manufactured by anodic aluminum oxide template on dye-sensitized solar cells. *Materials* **2017**, *10*, 296. [[CrossRef](#)]
12. Liu, Y.; Lin, Y.; Wei, Y.; Liu, C. Formation of carriers in Ti-oxide thin films by substitution reactions. *J. Appl. Phys.* **2012**, *111*, 043103. [[CrossRef](#)]

13. Zhang, S.; Zhang, X.; Sun, Y.; Zhou, W.; Cao, W.; Cheng, D. Investigation of the annealing treatment on the performance of TiO₂ photoanode. *Int. J. Hydrogen Energy* **2023**, *48*, 29996–30005. [[CrossRef](#)]
14. Phadke, S.; Du Pasquier, A.; Birnie, D.P., III. Enhanced electron transport through template-derived pore channels in dye-sensitized solar cells. *J. Phys. Chem. C* **2011**, *115*, 18342–18347. [[CrossRef](#)]
15. Wu, T.C.; Huang, W.M.; Meen, T.H.; Tsai, J.K. Performance improvement of dye-sensitized solar cells with pressed TiO₂ nanoparticles layer. *Coatings* **2023**, *13*, 907. [[CrossRef](#)]
16. Kim, M.H.; Kwon, Y.U. Semiconductor CdO as a blocking layer material on DSSC electrode: Mechanism and application. *J. Phys. Chem. C* **2009**, *113*, 17176–17182. [[CrossRef](#)]
17. Wang, J.; Wang, J.; Ding, J.; Wei, Y.; Zhang, J. Preparation of ZnO compact layer using vacuum ultraviolet for dye-sensitized solar cells. *Solid State Sci.* **2022**, *127*, 106860. [[CrossRef](#)]
18. Jadhav, V.S.; Bhande, S.S.; Tehare, K.K.; Gaikwad, S.L.; Mane, R.S. Significance of compact layers on DSSCs performance of chemically deposited TiO₂-based dye-sensitized solar cells. *Int. J. Eng. Sci.* **2015**, *4*, 30–34.
19. Hanaor, D.A.; Sorrell, C.C. Review of the anatase to rutile phase transformation. *J. Mater. Sci.* **2011**, *46*, 855–874. [[CrossRef](#)]
20. Li, J.; Zhang, H.; Wang, W.; Qian, Y.; Li, Z. Improved performance of dye-sensitized solar cell based on TiO₂ photoanode with FTO glass and film both treated by TiCl₄. *Phys. B Condens. Matter* **2016**, *500*, 48–52. [[CrossRef](#)]
21. Omar, A.; Abdullah, H. Electron transport analysis in zinc oxide-based dye-sensitized solar cells: A review. *Renew. Sustain. Energy Rev.* **2014**, *31*, 149–157. [[CrossRef](#)]

Disclaimer/Publisher's Note: The statements, opinions and data contained in all publications are solely those of the individual author(s) and contributor(s) and not of MDPI and/or the editor(s). MDPI and/or the editor(s) disclaim responsibility for any injury to people or property resulting from any ideas, methods, instructions or products referred to in the content.